International Journal of Innovative Computing, Information and Control
Volume **11**, Number **1**, February **2015**

ICIC International ©2015 ISSN 1349-4198
pp. **189–201**

BLOOD VESSEL SEGMENTATION IN RETINAL IMAGES BY MORPHOLOGICAL OPERATIONS AND BY A NOVEL PIXEL TRACKING ALGORITHM

Isam S. Hameed, Helen Ocbagabir, Buket D. Barkana* and Burak Yildirim

Electrical Engineering Department
University of Bridgeport
221 University Ave., Bridgeport 06604, USA
*Corresponding author: bbarkana@bridgeport.edu

Received September 2013; revised January 2014

Abstract. *Diabetic retinopathy is the most common diabetic eye disease and a leading cause of blindness. Diagnosis of diabetic retinopathy at an early stage can be done through the segmentation of the blood vessels of retina. Many studies have been carried out in the last decade in order to obtain accurate blood vessel segmentation in retinal fundus images including supervised and unsupervised methods. Supervised methods provide higher accuracies however they require more calculation time and their performance completely depend on the training data. In this work, an unsupervised segmentation method is proposed for blood vessel segmentation. A new vessel strengthening method and pixel tracking algorithm are presented. The pixel tracking algorithm filters background artifacts that have similar characteristics with small and thin vessels while segmenting vessels. The proposed segmentation method eliminates the dependency on training data and decreases the processing time of segmentation process while achieving high accuracy rates. Its performance is evaluated by using the DRIVE and STARE databases and achieved an average accuracy of 94.02% for the DRIVE database and 95.43% for the STARE database. Our results demonstrated an average sensitivity of 71.74% and a specificity of 97.28% for the DRIVE database while it is 71% and 97.4% for the STARE database, respectively. The calculated sensitivity and specificity values for both databases also state that the proposed segmentation method is reliable.*

Keywords: Diabetic retinopathy (DR), Segmentation, Pixel tracking, Vessel strengthening

1. **Introduction.** Diabetic retinopathy is the most common diabetic eye disease and a leading cause of blindness [4,6,26,31]. The estimated rate of this disease in the United States is 40.3% for diabetic adults 40 years or older [9]. People with diabetes are at risk for developing diabetic retinopathy. Over the past decade, there have been many studies in developing algorithms for computerized fundus colour image analysis to detect vessel structure, optic disc, and certain characteristic features of DR [5]. The purpose of the present study is to develop an automatic vessel segmentation algorithm which is fast and reliable. Since diabetic retinopathy issue has grown in importance in the clinical field, it became very necessary to adopt an automatic retinal vessels segmentation which will help a lot in detection of the abnormalities and morphological changes of the retinal blood vessels, and assist ophthalmologists to make accurate and early diagnosing and screening [17]. Many studies have been carried out to obtain accurate blood vessel segmentation in retinal images. These studies can be divided into two groups as unsupervised (ruled-based) methods and supervised methods.

Unsupervised methods employ vessel tracking methods, morphological operations, matching filters, etc. in order to obtain the vasculature structure. Mendonça and Campilho [18] reported the highest average accuracies (0.9463 and 0.9479) on both databases among the unsupervised methods. Their method extracts the vessel centerlines, which are used as guidelines for the subsequent vessel filling phase. The vessel segmentation is obtained using an iterative region growing method that integrates the contents of several binary images resulting from vessel width dependent morphological filters. Chaudhuri et al. introduced an operator for feature extraction based on the optical and spatial characteristics of regions to be recognized. The gray-level profile of the cross section of a blood vessel was approximated by a Gaussian shaped curve. The idea of matched filter detection of signals was used to detect piecewise linear segments of blood vessels in these images. They reported an average accuracy using the DRIVE database as 0.8773 [2]. Cinsdikici and Aydin [3] proposed a hybrid model. The ant colony algorithm is used to overcome the deficiency of the matched filter. Hoover et al. proposed a rule-based method that it uses local and global vessel features cooperatively to segment the vessel network. Their method complements local vessel attributes with region-based attributes of the network structure. A piece of the blood vessel network is hypothesized by probing an area of the matched filter response image, iteratively decreasing the threshold. At each iteration, region-based attributes of the piece are tested to consider probe continuation and ultimately to decide if the piece is vessel. The performance of their method is evaluated using the STARE database, and their accuracy is reported as 0.9275 [11]. A general framework for model-based locally adaptive thresholding based on a verification-based multi-threshold probing scheme was presented by Jiang and Mojon [14]. This common methodology is enriched by incorporating relevant information related to retinal vessels into the verification process with the aim of enabling its application to retinal images. In terms of average accuracy, 0.8911 and 0.9009 were achieved on DRIVE and STARE databases, respectively.

Martinez-Perez et al. [17] proposed a method that achieves average accuracies of 0.9344 and 0.9410 using DRIVE and STARE databases, respectively. It is based upon multi-scale feature extraction. The local maxima over scales of the gradient magnitude and the maximum principal curvature of the Hessian tensor were used in a multiple pass region growing procedure. Growth progressively segmented the blood vessels by using both feature and spatial information. Some other rule-based methods can be found in [1,7,10,27,28,30].

Supervised methods are based on pixel classification, which consists on classifying each pixel into two classes, vessel and non-vessel, by using a feature set. The feature set contains parameters that are used to decide if a pixel is a part of a vessel or not. The dimension of the feature set affects the complexity and the accuracy of the classifier. Generally, supervised methods outperform rule-based methods. However, they might require more computation time because of their complexity. Some important studies proposing a supervised method can be found in [16,19,21,22,24,25].

Unsupervised methods use matching filters, local adaptive thresholding methods, morphological techniques, or detecting the vessels through special tracking methods while supervised methods use classifiers to decide whether the processed pixel is a vessel or non-vessel. A detailed review, analysis, and categorization of the retinal vessel extraction algorithms can be found in the work of Fraz et al. [32]. Supervised methods are more complex than unsupervised methods which lead to make them slower due to their complexity. In addition, the performance of supervised methods completely depends on the training data making the segmentation accuracy unreliable for unknown retinal image databases. For these reasons, we propose an unsupervised method which has less processing time and

power consumption while achieving the same or higher level of accuracy with supervised methods for retinal vessel segmentation.

2. **Image Databases.** For the evaluation of the proposed retinal vessel segmentation method, two publicly available retinal image databases, DRIVE [20] and STARE [12], are used.

The DRIVE (Digital Retinal Images for Vessel Extraction) database contains forty eye-fundus color images (with and without present pathology) and their ground truth images. All images in DRIVE database are digitized by using a Canon CR5 non-mydriatic 3CCD camera with a 45 field-of-view (FOV). Each image is captured using 8 bits per color-channel at the image size of 565×584 pixels, and each was originally saved in JPEG format. Two ground truth vessel segmentation results were produced by two different experts for each image. The first expert's results are used to test our method.

The STARE database, originally collected by Hoover et al. [11], contains twenty retinal fundus slides (ten of them contain pathology) and their ground truth images. The images are digitalized by a TopCon TRV-50 fundus camera with 35 degree FOV. Each slide is digitized to produce a 605×700 pixel image with 8 bits per color-channel and is available in the PPM format. All the twenty images are carefully labeled by hand to produce ground truth vessel segmentation by an expert. The database contains two sets of ground truth made by two different experts. First expert's ground truth results are used to test our method.

3. **Methodology.** The framework of the proposed method is given in Figure 1. It is divided into three main stages. a) Pre-processing; b) Vessel strengthening; c) Star network pixel tracking algorithm and segmentation.

3.1. **Preprocessing.** Retinal fundus images have low contrast and sometimes noisy backgrounds. Therefore, blood vessels, especially the small and thin vessels need to be enhanced before the segmentation process. Pre-processing stage performs green channel extraction, global vessel enhancement, and image de-noising.

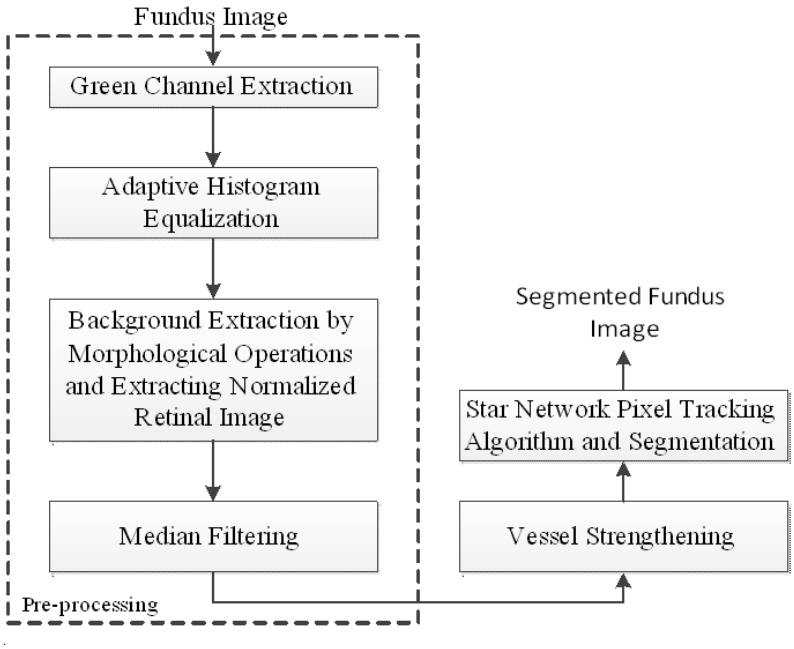

FIGURE 1. The framework of the proposed method

Green channel extraction: It is stated that the green channel of the retinal images contains more details about the vessel structure which are needed to be segmented. Red and blue channels do not provide as clear images of blood vessels as green channel and this is due to low contrast and poor dynamic range. Red channel provides brighter image with low contrast and blue channel gives a poor dynamic range. It makes the green channel as the best choice for its higher contrast and best represented vessels [29].

Global vessel enhancement: Adaptive histogram equalization (AHE) is used since it tends to enhance the contrast level of an image by uniformly spreading the image intensity levels. Figure 2(a) shows the image after AHE is applied.

AHE is applied to the compliment of the green channel to enhance the vessels. AHE is considered as a powerful way of adjusting the intensity values of a digital image. It works on specific small areas in the image, usually called tiles, rather than applying the process on the entire image, i.e., instead of processing the entire retinal image with its noisy background AHE intends to uniformly enhance the image by processing small regions individually [13].

Morphological methodology with image de-noising: Morphological operations are used to create a uniform background image. As it can be seen in Figure 2(a), the background became non-uniform after the AHE stage while the vessel structure got a better contrast. The most basic morphological operations are erosion and dilation [15]. Both processes are controlled by a binary array that is called structuring element. The structuring element is known as a matrix with values 1 and 0 only, and takes different shapes and sizes with respect to the application. Erosion refers to the process of trimming or thinning the pixels in the digital images. Dilation refers to the process of expanding the pixels in the digital image which results in growing the processed area in the image [8,23]. Mathematically, Equation (1) and Equation (2) express erosion and dilation operations, respectively.

$$A \ominus B = \{z : (B)_z \cap A^c \neq \varnothing\} \tag{1}$$

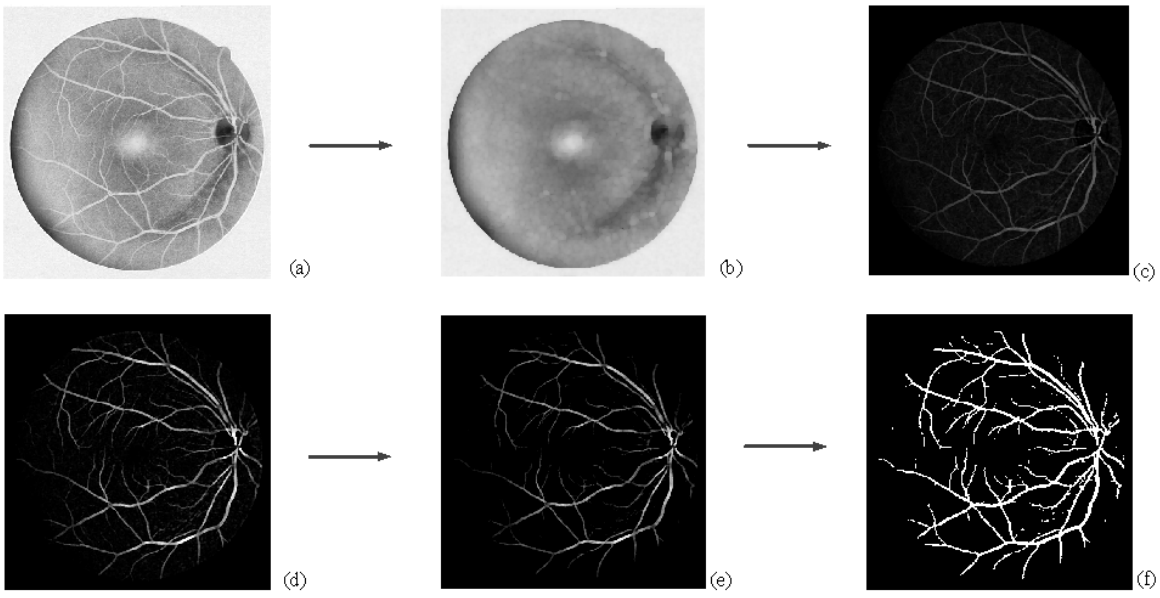

FIGURE 2. (a) Adaptive histogram equalization, (b) created background by a 6×6 ball-shaped structuring element (image), (c) normalized retinal image (image), (d) strengthened image, (e) the result of the star network pixel tracking algorithm in grayscale, (f) segmented retinal blood vessels

$$A \oplus B = \{z : (B^{\wedge})_z \cap A \neq \varnothing\} \tag{2}$$

where, $A \ominus B$ is the erosion of image A with a structuring element B, $(B)_z$ is the translated structuring element, and A^c is the complement of the image A. And, $A \oplus B$ is the dilation of image A with a structuring element B, and $(B^{\wedge})_z$ is the reflected and translated structuring element B. The erosion followed by dilation is called, *image opening*. It is defined by Equation (3).

$$A \circ B = (A \ominus B) \oplus B \tag{3}$$

where, $A \circ B$ refers to the morphological opening process [8]. The blood vessels are suppressed by an 'opening' operation with a structuring element that is non-flat and 6×6 ball-shaped, to create a background image, I_{BK}. This background image is used to get a normalized image, I_{NR}. The result of the AHE, I_{ADT}, is subtracted from the created background I_{BK} in order to obtain a normalized image I_{NR}. The normalized image is found by Equation (4).

$$I_{NR}(x, y) = median filter \{I_{ADT}(x, y) - I_{BK}(x, y)\} \tag{4}$$

Median filtering is applied to remove salt-and-pepper noise. The created background and normalized image can be seen in Figures 2(b) and 2(c).

3.2. **Vessels strengthening.** In common, large retinal vessels show higher intensity values than the small retinal vessels during fundus camera image capturing [30]. As confirming this fact, it has been observed that the normalized retinal image, I_{NR}, has an intensity variations between the thick and small retinal vessels. Hence, we propose an algorithm to strengthen the intensity levels of the thin and small vessels while keeping the intensity levels of background unchanged. It is performed by a set of morphological operations. The normalized retinal image (Figure 2(c)) is opened to create a background, I_{BK1}. Next, normalized retinal image, I_{NR1}, is created by subtracting I_{BK1} from I_{NR}. I_{NR1} will be opened again, and the resulting background, I_{BK2}, is subtracted from I_{NR1} to obtain I_{NR2}. I_{NR} and I_{NR2} are added to create an image, I_{NR3}, with improved vessel structure. The subtraction of I_{BK4} and I_{BK5} from I_{NR5} and I_{NR6} generates the strengthened image in Figure 2(d). Equations (5)-(11) define the vessel strengthen algorithm mathematically. The algorithm is also given as a flowchart in Figure 3.

$$I_{NR1}(x, y) = I_{NR}(x, y) - I_{BK1}(x, y) \tag{5}$$

$$I_{NR2}(x, y) = I_{NR1}(x, y) - I_{BK2}(x, y) \tag{6}$$

$$I_{NR3}(x, y) = I_{NR}(x, y) + I_{NR2}(x, y) \tag{7}$$

$$I_{NR4}(x, y) = I_{NR3}(x, y) - I_{BK3}(x, y) \tag{8}$$

$$I_{NR5}(x, y) = I_{NR2}(x, y) + I_{NR4}(x, y) \tag{9}$$

$$I_{NR6}(x, y) = I_{NR5}(x, y) - I_{BK4}(x, y) \tag{10}$$

$$I_{NR7}(x, y) = I_{NR6}(x, y) - I_{BK5}(x, y) \tag{11}$$

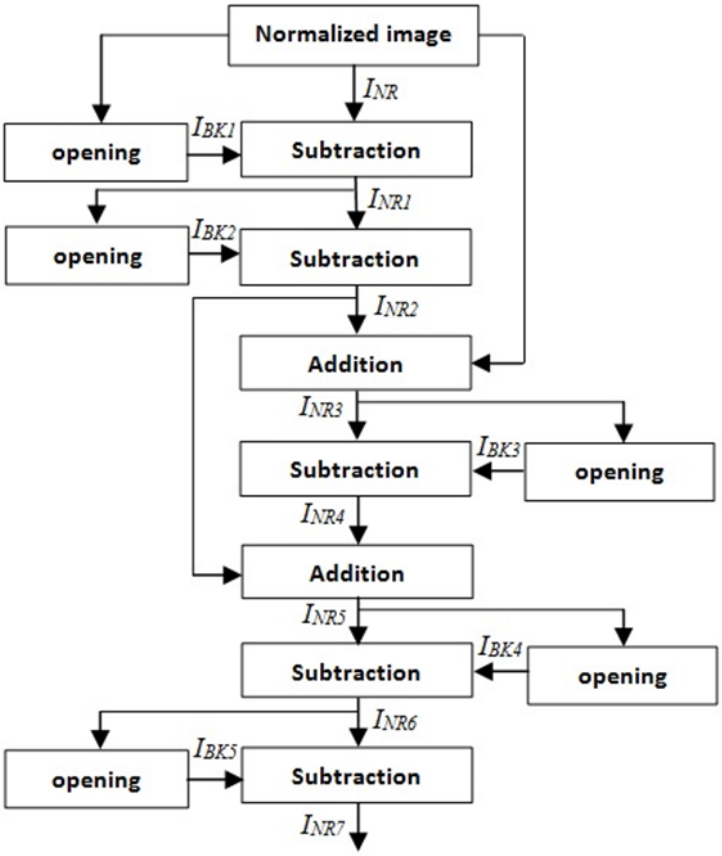

FIGURE 3. The vessel strengthening algorithm

3.3. **Star network pixel tracking algorithm.** Star network pixel tracking algorithm can be defined as an unsupervised classification method. This algorithm depends on the basic morphology of the retinal vessel tree represented by vessels' continuous connection starting from the optic disk. Pixels are tracked one by one throughout the entire image by inspecting its neighborhoods in order to make a decision whether the processed pixel is a part of a vessel. If the decision is positive, the processed pixel is set to "1", otherwise it is set to intensity value of "0". This algorithm is able to distinguish and remove the artifacts that are aligned in the same fashion as small vessels. The tracking process goes over the entire image by comparing each pixel with its four neighboring pixels aligned at 45° to each other. An illustration of the star network pixel tracking algorithm is shown in Figure 4.

The star network pixel tracking algorithm can be summarized as the following steps.

Step 1: Four pixels in eight directions are checked separately if they are connected or not.

Step 2: Once four pixels in any direction are found to be connected, the checking process takes the last pixel in that direction as new processed pixel.

Step 3: Step 1 is applied to the new processed pixel. In this case, only seven directions are taken in consideration since the direction which the new processed pixel came from has been already processed.

Step 4: Eight pixels are checked if they are connected. If the pixels are connected the processed pixel is set to 1 as a part of the vessel structure. Otherwise, the pixel is set to zero representing that the processed pixel is not a part of the vessel structure.

Step 5: Steps from 2 to 4 are repeated until all image is processed.

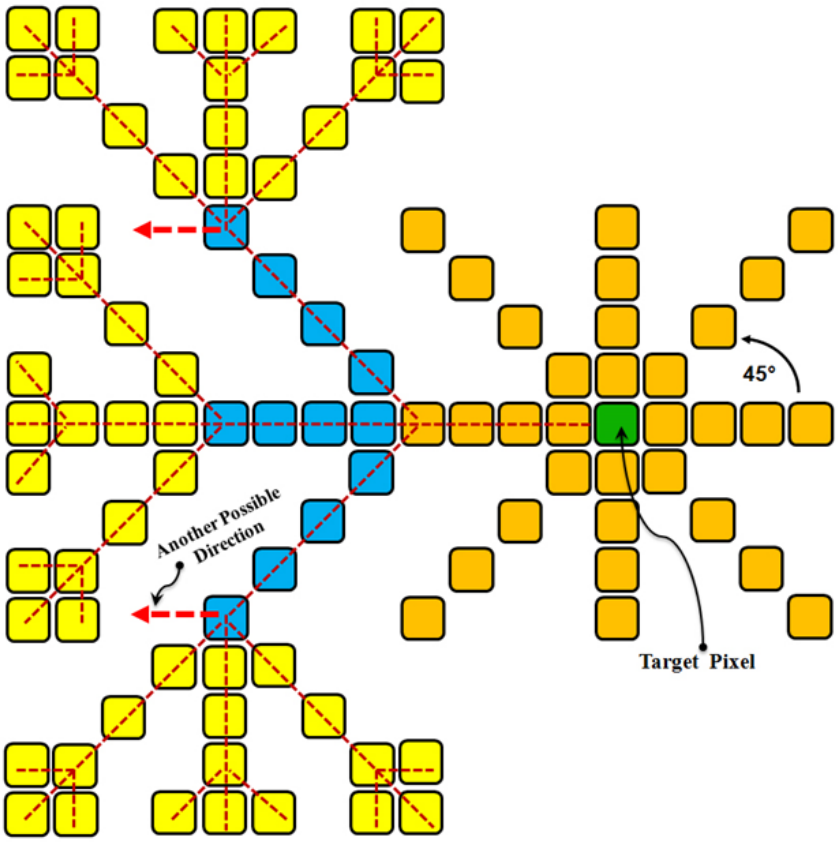

FIGURE 4. The star network pixel tracking algorithm

Figure 2(e) shows the results of this algorithm in grayscale. It can be seen that the pixel tracking algorithm filters background artifacts that have similar characteristics with small and thin vessels while segmenting vessels. Figure 2(f) presents the segmented retinal blood vessels by the star network pixel tracking algorithm.

Figure 5 shows the results of the proposed methods step by step for two images of the DRIVE and STARE databases. Figures (a)-(f) present results with the lowest accuracy, and figures (g)-(l) present results with the highest accuracy for both databases.

4. **Results and Discussion.**

4.1. **Performance measures.** To compare the performance of the proposed segmentation method with previous methods, we used public domain DRIVE and STARE databases. The performance of our unsupervised method is only evaluated on the test image set to prevent bias between supervised and unsupervised vessel segmentation methods. For each feature set, segmentation result is compared to ground truth data. Accuracy (Acc), sensitivity (Se), specificity (Sp), positive predictive value (Ppv), and negative predictive value (Npv) are calculated. These are defined as

$$Acc = (TP + TN)/(TP + FN + TN + FP) \tag{12}$$

$$Se = TP/(TP + FN) \tag{13}$$

$$Sp = TN/(TN + FP) \tag{14}$$

$$Npv = TN/(TN + FN) \tag{15}$$

$$Ppv = TP/(TP + FP) \tag{16}$$

where TP is the number of positive cases correctly classified as positive; TN is the number of the cases correctly classified as negative; FN is the number of positive cases classified as negative; and FN is the number of negative cases classified as positive. Table 1 and Table 2 present the performance results of the proposed method.

The receiver operating characteristic (ROC) curve analysis is also performed. The ROC analysis is appropriate for two-class segmentation applications and it becomes common to use ROC to evaluate the performance of segmentation methods. To build an ROC curve, a set of threshold values are chosen and, for each of these, the true positive ratio (y-axis) and false positive ratio (x-axis) values are calculated and plotted against each other. The true positive ratio is defined as sensitivity and the false positive ratio is defined as 1-specificity. The entire test images from both databases are analyzed and the average ROC curves are plotted in Figure 6.

Table 3 compares this work with previous methods [2,3,11,14,17,18] and [16,19,21,24,25].

The method achieved an accuracy rate of 94.02% and 95.43% for the DRIVE and STARE databases, respectively. The accuracy of our algorithm surpasses the most of the previous unsupervised methods. It is known that supervised methods often outperform unsupervised methods. However, supervised methods may show significant performance loss when applied to a different database. Their accuracy significantly worsens when

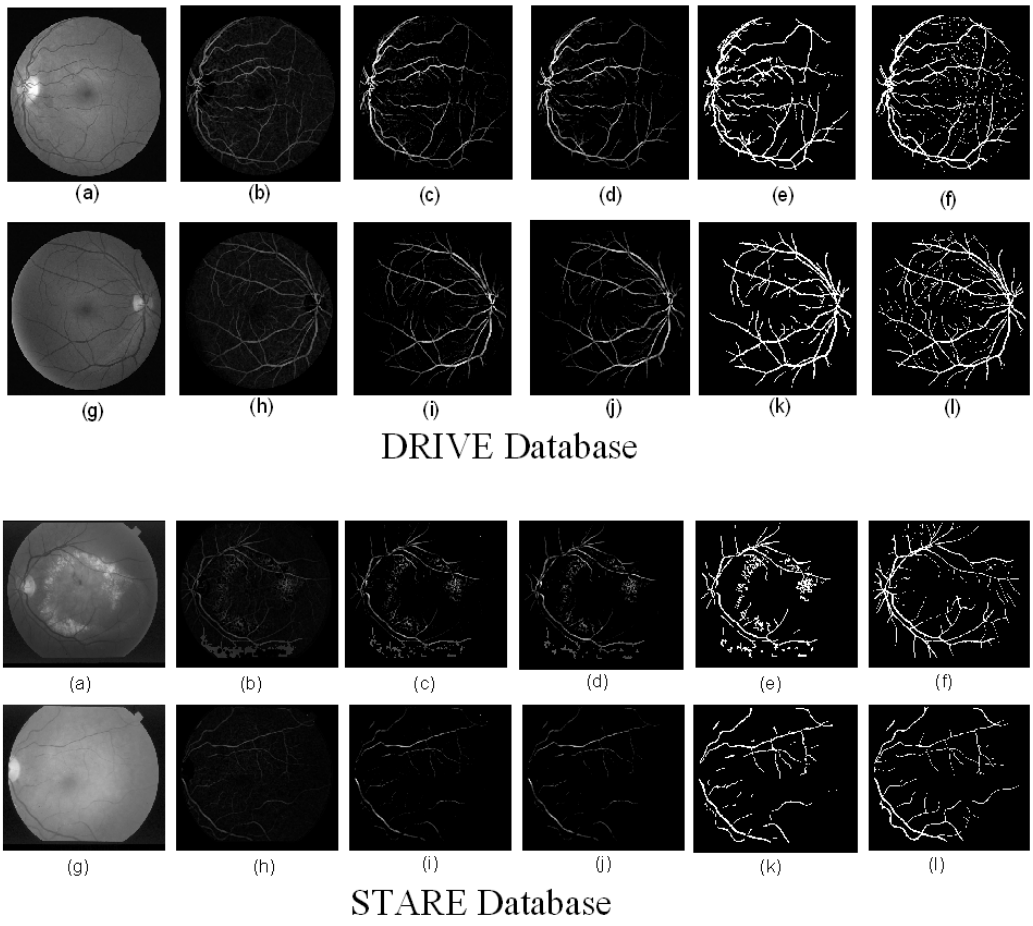

FIGURE 5. DRIVE and STARE databases (a and g) green channel images, (b and h) normalized images, (c and i) strengthened images, (d and j) star network pixel tracking algorithm results in grayscale, (e and k) segmentation results, (f and l) ground truth images

TABLE 1. Performance results on DRIVE database images

Image	Accuracy	Sensitivity	Specificity	Ppv	Npv	AUC
#1	0.9420	0.8151	0.9611	0.7600	0.9718	0.9182
#2	0.9402	0.8091	0.9633	0.7958	0.9662	0.9149
#3	0.9330	0.6744	0.9772	0.8343	0.9462	0.8640
#4	0.9436	0.7215	0.9777	0.8331	0.9580	0.8759
#5	0.9414	0.6555	0.9863	0.8827	0.9480	0.8495
#6	0.9371	0.6319	0.9873	0.8912	0.9423	0.8416
#7	0.9333	0.7000	0.9689	0.7743	0.9549	0.8644
#8	0.9350	0.5930	0.9843	0.8446	0.9437	0.8271
#9	0.9455	0.6199	0.9888	0.8807	0.9413	0.8364
#10	0.9460	0.6920	0.9804	0.8275	0.9591	0.8664
#11	0.9252	0.7514	0.9511	0.6961	0.9625	0.8807
#12	0.9441	0.7155	0.9768	0.8155	0.9600	0.8783
#13	0.9360	0.6856	0.9773	0.8332	0.9495	0.8632
#14	0.9433	0.7754	0.9658	0.7523	0.9698	0.9022
#15	0.9327	0.7780	0.9506	0.6462	0.9737	0.8954
#16	0.9413	0.7339	0.9726	0.8010	0.9604	0.8835
#17	0.9397	0.6763	0.9767	0.8033	0.9555	0.8592
#18	0.9392	0.7706	0.9610	0.7196	0.9700	0.8963
#19	0.9552	0.8243	0.9732	0.8078	0.9759	0.9205
#20	0.9498	0.7265	0.9764	0.7861	0.9676	0.8868
Ave	**0.9402**	**0.7174**	**0.9728**	**0.7993**	**0.9588**	**0.8762**

TABLE 2. Performance results on STARE database images

Image	Accuracy	Sensitivity	Specificity	Ppv	Npv	AUC
#1	0.9434	0.5929	0.9737	0.6620	0.9650	0.8588
#2	0.9374	0.5314	0.9663	0.5297	0.9666	0.8218
#3	0.9385	0.7701	0.9492	0.4913	0.9848	0.9131
#4	0.9404	0.2439	0.9961	0.8346	0.9427	0.7195
#5	0.9507	0.7816	0.9675	0.7051	0.9781	0.9268
#6	0.9670	0.7727	0.9816	0.7582	0.9830	0.9122
#7	0.9461	0.9113	0.9491	0.6094	0.9919	0.9604
#8	0.9552	0.8985	0.9597	0.6430	0.9915	0.9586
#9	0.9545	0.8739	0.9614	0.6591	0.9889	0.9523
#10	0.9571	0.8145	0.9695	0.7005	0.9835	0.9412
#11	0.9557	0.8416	0.9645	0.6452	0.9876	0.9442
#12	0.9599	0.8978	0.9651	0.6834	0.9912	0.9601
#13	0.9562	0.7873	0.9727	0.7384	0.9791	0.9226
#14	0.9568	0.7752	0.9749	0.7544	0.9775	0.9232
#15	0.9565	0.7746	0.9737	0.7353	0.9786	0.9227
#16	0.9464	0.6053	0.9852	0.8229	0.9564	0.859
#17	0.9647	0.8101	0.9799	0.7986	0.9813	0.9378
#18	0.9742	0.5677	0.9959	0.8806	0.9774	0.8528
#19	0.9743	0.5334	0.9942	0.8055	0.9793	0.8721
#20	0.9517	0.4166	0.9900	0.7489	0.9596	0.7961
Ave	**0.9543**	**0.7100**	**0.9740**	**0.7103**	**0.9772**	**0.8978**

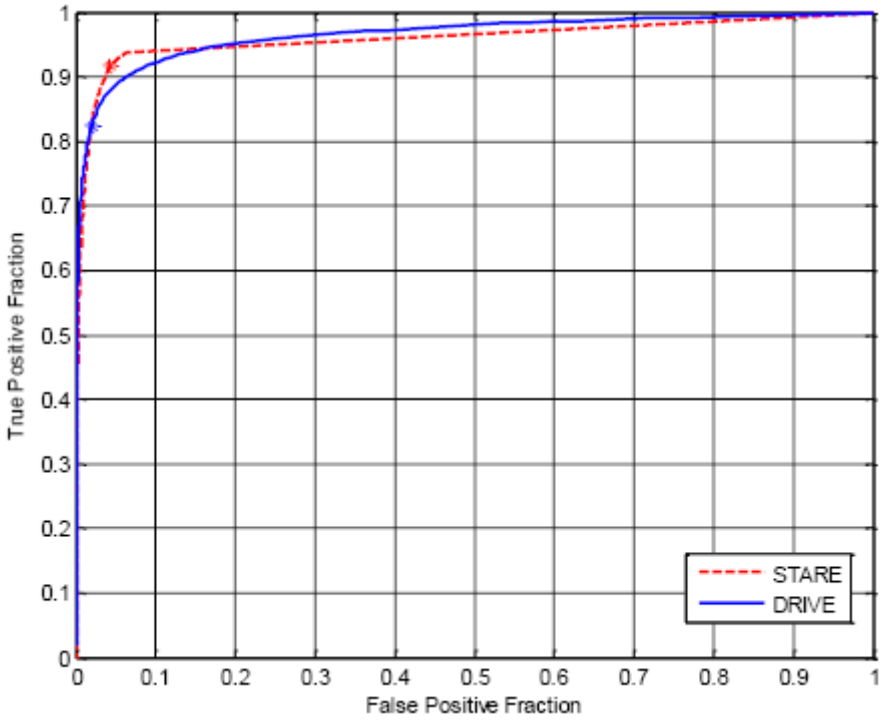

FIGURE 6. ROC curves for the DRIVE and STARE databases (Image #19 from DRIVE and Image #12 from STARE databases)

TABLE 3. Performance results compared to other methods on the DRIVE and STARE databases in terms of average accuracy and area under ROC curve (AUC)

Type	**Method**	**DRIVE Accuracy and (*AUC*)**	**STARE Accuracy and (*AUC*)**
Unsupervised (Rule-Based) Methods	Chaudhuri *et al.* [2]	0.8773 (*0.7878*)	–
	Hoover *et al.* [11]	–	0.9275 (*0.7590*)
	Jiang and Mojon [14]	0.8911 (*0.9327*)	0.9009 (*0.9298*)
	Mendonça and Campilho [18]	0.9463 (*NA*)	0.9479 (*NA*)
	Martinez-Perez *et al.* [17]	0.9344 (*NA*)	0.9410 (*NA*)
	Cinsdikici and Aydin [3]	0.9293 (*0.9407*)	–
	This work	**0.9402 (*0.8762*)**	**0.9543 (*0.8977*)**
Supervised Methods	Staal *et al.* [25]	0.9441 (*0.9520*)	–
	Niemeijer *et al.* [19]	0.9417 (*0.9294*)	–
	Soares *et al.* [24]	0.9466 (*0.9614*)	0.9480 (*0.9671*)
	Ricci and Perfetti [21]	0.9595 (*0.9633*)	0.9646 (*0.9680*)
	Marín *et al.* [16]	0.9452 (*0.9588*)	0.9526 (*0.9769*)

the method is trained and tested on a different database. This is a disadvantage for practical applications since a blood vessel detection tool must be robust and work on retinal images from multiple origins, and it must perform well when it is used by different operators working with different equipment. Our results demonstrated a sensitivity of 71.74% and a specificity of 97.28% for the DRIVE database while it is 71% and 97.4% for the STARE database, respectively. The calculated sensitivity and specificity values for both databases state that the proposed segmentation method is reliable and robust.

Another important measure of the performance of a method is the area under the curve (AUC). It can take values from 0.0 to 1.0. Table 3 also presents the average AUC values for our method and for the previous works.

A summary of the segmentation results on DRIVE database images (Table 2) shows that the proposed method reaches better accuracy rate than all unsupervised methods except Mendonça and Campilho [18]. Mendonça and Campilho did not report their AUC values. All supervised methods slightly achieved higher accuracy rates than our method except Ricci and Perfetti [21]. Regarding STARE database, the proposed method delivered higher accuracy rates than the unsupervised methods in the literature.

5. **Conclusions.** In this paper, an unsupervised method is proposed for blood vessel segmentation in retinal images. Unsupervised classification is more challenging than supervised classification. In most cases, supervised classification is the preferable option if it is possible. However, it is needed to resort to unsupervised methods if the feature vector describing an object can be expected to change with time or subject. Blood vessel structure in retinal images is different for each subject. Therefore, unsupervised classification methods in this field gain an importance.

A new vessel strengthening method and pixel tracking algorithm are proposed. The vessel strengthening method strengthens the intensity levels of the thin and small vessels while keeping the intensity levels of background unchanged. It is performed by a set of morphological operations. The pixel tracking algorithm cleans the background noise that show similar characteristics with small and thin vessels. It can be defined as an unsupervised classification method and depends on the basic morphology of the retinal vessel tree represented by vessels' continuous connection starting from the optic disk. Pixels are tracked one by one throughout the entire image by inspecting its neighborhoods in order to make a decision whether the processed pixel is a part of a vessel.

The performance of our method is tested by using the DRIVE and STARE databases like the previous studies in the literature. Our method achieved high accuracy rates (94.02% for DRIVE and 95.43% for STARE) among unsupervised methods while avoiding heavy computation and human supervision. The total processing time of a single image is less than 10 seconds, running on a PC with an Intel(R) Core(TM) i3 CPU at 2.53 GHz and 3 GB of RAM.

Acknowledgment. The authors would like to thank the authors of DRIVE and STARE databases for making their data publicly available.

REFERENCES

[1] M. U. Akram, I. Jamal, A. Tariq and J. Imtiaz, Automated segmentation of blood vessels for detection of proliferative diabetic retinopathy, *Proc. of the Int. Conference IEEE-EMBS Biomedical and Health Informatics*, pp.232-235, 2012.

[2] S. Chaudhuri, S. Chatterjee, N. Katz, M. Nelson and M. Goldbaum, Detection of blood vessels in retinal images using two-dimensional matched filters, *IEEE Trans. Med. Imag.*, vol.8, no.3, pp.263-269, 1989.

[3] M. G. Cinsdikici and D. Aydin, Detection of blood vessels in ophthalmoscope images using MF/ant (matched filter/ant colony) algorithm, *Comput Methods Programs Biomed.*, vol.96, pp.85-95, 2009.

[4] T. Dall, S. E. Mann, Y. Zhang, J. Martin, Y. Chen and P. Hogan, Economic costs of diabetes in the U.S. in 2007, *Diabetes Care: American Diabetes Association*, vol.31, pp.596-615, 2008.

[5] B. Dupas, T. Walter, A. Erginay, R. Ordonez, N. Deb-Joardar, P. Gain, J. C. Klein and P. Massin, Evaluation of automated fundus photograph analysis algorithms for detecting microaneurysms, haemorrhages and exudates, and of a computer-assisted diagnostic system for grading diabetic retinopathy, *Diabetes & Metabolism*, vol.36, pp.213-220, 2010.

[6] M. H. A. Fadzil, L. I. Izhar, H. Nugroho and H. A. Nugroho, Analysis of retinal fundus images for grading of diabetic retinopathy severity, *Med. Biol. Eng. Comput.*, vol.49, pp.693-700, 2011.
[7] L. Gagnon, M. Lalonde, M. Beaulieu and M. C. Boucher, Procedure to detect anatomical structures in optical fundus images, *Proc. of the SPIE Med Imag: Image Process*, pp.1218-1225, 2001.
[8] R. Gonzalez, R. Woods and S. Eddins, *Digital Image Processing Using MATLAB*, 2nd Edition, Gatesmark Publishing, USA, 2009.
[9] C. E. Hann, J. A. Revie, D. Hewett, J. G. Chase and G. M. Shaw, Screening for diabetic retinopathy using computer vision and physiological markers, *J. Diabetes Science and Technology*, vol.3, no.1, pp.819-834, 2009.
[10] C. Heneghan, J. Flynn, M. O'Keefe and M. Cahill, Characterization of changes in blood vessel width and tortuosity in retinopathy of prematurity using image analysis, *Med. Image Anal.*, vol.6, pp.407-429, 2002.
[11] A. Hoover, V. Kouznetsova and M. Goldbaum, Locating blood vessels in retinal images by piecewise threshold probing of a matched filter response, *IEEE Trans. Med. Imag.*, vol.19, no.3, pp.203-210, 2000.
[12] A. Hoover, *STARE Database*, http://www.ces.clemson.edu/∼ahoover/stare.
[13] F. Hossain and M. R. Alsharif, Image enhancement based on logarithmic transform coefficient and adaptive histogram equalization, *Proc. of the Int. Conf. Convergence Information Technology*, pp.1439-1444, 2007.
[14] X. Jiang and D. Mojon, Adaptive local thresholding by verificationbased multithreshold probing with application to vessel detection in retinal images, *IEEE Trans. Pattern Anal. Mach. Intell.*, vol.25, no.1, pp.131-137, 2003.
[15] P. Jitpakdee, P. Aimmanee and B. Uyyanonvara, A survey on hemorrhage detection in diabetic retinopathy retinal images, *Proc. of the 9th Int. Conf. Electrical Engineering/Electronics, Computer, Telecommunications and Information Technology (ECTI-CON)*, pp.1-4, 2012.
[16] D. Marín, A. Aquino, M. E. Gegundez-Arias and J. M. Bravo, A new supervised method for blood vessel segmentation in retinal images by using gray-level and moment invariants-based features, *IEEE Trans. Med. Imag.*, vol.30, no.1, pp.146-158, 2011.
[17] M. E. Martinez-Perez, A. D. Hughes, S. A. Thom, A. A. Bharath and K. H. Parker, Segmentation of blood vessels from red-free and fluorescein retinal images, *Med. Imag. Anal.*, vol.11, pp.47-61, 2007.
[18] M. Mendonça and A. Campilho, Segmentation of retinal blood vessels by combining the detection of centerlines and morphological reconstruction, *IEEE Trans. Med. Imag.*, vol.25, no.6, pp.1200-1213, 2006.
[19] M. Niemeijer, J. Staal, B. V. Ginneken, M. Loog and M. D. Abramoff, Comparative study of retinal vessel segmentation methods on a new publicly available database, *Proc. of the SPIE Med. Imag.*, vol.5370, pp.648-656, 2004.
[20] *Research Section, Digital Retinal Image for Vessel Extraction, (DRIVE) Database. Utrecht*, The Netherlands, Univ., Med. Center Utrecht, Image Sci. Inst., http://www.isi.uu.nl/Re-search/Data bases/DRIVE.
[21] E. Ricci and R. Perfetti, Retinal blood vessel segmentation using line operators and support vector classification, *IEEE Trans. Med. Imag.*, vol.26, no.7, pp.1357-1365, 2007.
[22] D. Selvathi and N. Balagopal, Detection of retinal blood vessels using curvelet transform, *Proc. of the Int. Conf. Devices Circuits and Systems*, pp.325-329, 2012.
[23] J. Semmlow, *Biosignal and Medical Image Processing*, 2nd Edition, CRC Press, New York, 2008.
[24] J. V. B. Soares, J. J. G. Leandro, R. M. Cesar Jr, H. F. Jelinek and M. J. Cree, Retinal vessel segmentation using the 2D Gabor wavelet and supervised classification, *IEEE Trans. Med. Imag.*, vol.25, no.6, pp.1214-1222, 2006.
[25] J. Staal, M. D. Abràmoff, M. Niemeijer, M. A. Viergever and B. van Ginneken, Ridge based vessel segmentation in color images of the retina, *IEEE Trans. Med. Imag.*, vol.23, no.1, pp.501-509, 2004.
[26] C. R. Taylor, L. M. Merin, A. M. Salunga, J. T. Hepworth, T. D. Crutcher, D. M. O'Day and B. A. Pilon, Improving diabetic retinopathy screening ratios using telemedicine-based digital retinal imaging technology: The Vine Hill study, *Diabetes Care*, vol.30, no.3, pp.574-578, 2007.
[27] Y. A. Tolias and S. M. Panas, A fuzzy vessel tracking algorithm for retinal images based on fuzzy clustering, *IEEE Trans. Med. Imag.*, vol.17, no.2, pp.263-273, 1998.
[28] D. Vallabha, R. Dorairaj, K. Namuduri and H. Thompson, Automated detection and classification of vascular abnormalities in diabetic retinopathy, *Proc. of the 38th Int. Conf. Signals, Systems and Computers*, vol.2, pp.1625-1629, 2004.

[29] T. Walter, P. Massin, A. Erginay, R. Ordonez, C. Jeulin and J. C. Klein, Automatic detection of microaneurysms in color fundus images, *Med. Image Anal.*, vol.11, pp.555-566, 2007.

[30] L. Xu and S. Luo, A novel method for blood vessel detection from retinal images, *BioMedical Engineering*, pp.9-14, 2010.

[31] X. Zhang, J. B. Saaddine, C. F. Chou, M. F. Cotch, Y. J. Cheng, L. S. Geiss, E. W. Gregg, A. L. Albright, B. E. K. Klein and R. Klein, Prevalence of diabetic retinopathy in the United States 2005-2008, *JAMA*, vol.304, no.3, pp.649-656, 2010.

[32] M. M. Fraz, P. Remagnino, A. Hoppe, B. Uyyanonvara, A. R. Rudnicka, C. G. Owen and S. A. Barman, Blood vessel segmentation methodologies in retinal images – A survey, *Computer Methods and Programs in Biomedicine*, vol.108, no.1, pp.407-433, 2012.